RSC Advances

PAPER

View Article Online
View Journal | View Issue

Cite this: *RSC Adv.*, 2015, **5**, 89218

Two blue iridium complexes for efficient electroluminescence with low efficiency roll-off†

Qiu-Lei Xu, Xiao Liang, Liang Jiang, Yue Zhao and You-Xuan Zheng*

Received 26th July 2015
Accepted 12th October 2015

DOI: 10.1039/c5ra14837e

www.rsc.org/advances

Two bis-cyclometalated iridium complexes ($(dfpypy)_2Ir(tpip)$ and $(dfpypy)_2Ir(Ftpip)$) with fluorinated substituted bipyridine (2′,6′-difluoro-2,3′-bipyridine, dfpypy) as the main ligand and tetraphenylimidodiphosphinate derivatives (tpip and Ftpip) as the ancillary ligands were prepared, and their X-ray crystallographic, photoluminescence and electrochemical properties were investigated. The $(dfpypy)_2Ir(tpip)$ and $(dfpypy)_2Ir(Ftpip)$ complexes showed blue emission at 457 nm with quantum efficiency yields of 7.0% and 7.1%, respectively. Organic light emitting diodes (OLEDs) with the structure of ITO/TAPC (1,1-bis[4-(di-*p*-tolylamino)phenyl]cyclohexane, 40 nm)/mCP (1,3-bis(9*H*-carbazol-9-yl) benzene, 10 nm)/$(dfpypy)_2Ir(tpip)$ or $(dfpypy)_2Ir(Ftpip)$ (8 wt%): PPO21 (3-(diphenylphosphoryl)-9-(4-(diphenylphosphoryl)phenyl)-9*H*-carbazole, 25 nm)/TmPyPB (1,3,5-tri(*m*-pyrid-3-yl-phenyl)benzene, 50 nm)/LiF (1 nm)/Al (100 nm) (**B2** and **B3**) exhibit performances with the maximum current efficiency (η_c) values of 22.83 and 20.79 cd A^{-1}, respectively, with low efficiency roll-off. For example, at 100 cd m^{-2} display brightness, the current efficiencies of devices **B2** and **B3** are 19.78, 13.74 cd A^{-1}, respectively. At 1000 cd m^{-2} light brightness, these values are still 20.39 and 20.75 cd A^{-1}, respectively. Even at the high luminance of 5000 cd m^{-2}, these data also remained at 19.95 and 20.08 cd A^{-1}, respectively.

Introduction

Phosphorescent iridium complexes have been widely used as dopants in organic light-emitting diodes (OLEDs) due to their high quantum efficiency, broad emission range and short triplet exited state lifetime.[1] To achieve full color display, three primary color (blue, green and red) emitters are needed. However, compared with green and red complexes, efficient blue phosphorescent materials are still limited for stable OLEDs. Thus, it is still necessary to develop new efficient blue phosphorescent compounds to satisfy the high demand of the display and lighting industry.

Typically, 2-phenylpyridine derivatives were widely used as the main ligands for blue Ir(III) emitters. It was easy to control the emission spectra as the modification of phenyl unit with electron-drawing group would lower the HOMO, while the modification of pyridine unit with electron-donating moiety can improve the LUMO level of the Ir(III) complexes. Usually, there are two ways to develop blue Ir(III) complexes: (i) the adorption of a main cyclometalated ligand with large triplet energy and (ii) the inducement of a larger band gap by stabilizing the highest occupied molecular orbital (HOMO) and destabilizing the lowest unoccupied molecular orbital (LUMO) level, since the emission energies of Ir(III) complexes are mainly dominated by the triplet energy of the C^N chelating ligand.

Iridium(III)bis(4,6-difluorophenyl-pyridinato)picolinate (FIrpic) was widely used as sky-blue dopant at 470 nm with two fluorine atoms in the phenyl unit to shift the HOMO level downward for high triplet energy.[2] Furthermore, several deep blue dopants with additional electron withdrawing substituent were reported such as FCNIr(pic) (iridium(III)bis((3,5-difluoro-4-cyanophenyl)-pyridine)picolinate), $(HFP)_2Ir(pic)$ (iridium(III)(bis(2-(2,4-difluoro-3-(perfluoropropyl)phenyl)-4-methylpyridine))picolinate) and so on.[3] Recently, fluorinated dipyridine ligand, 2′,6′-difluoro-2,3′-bipyridine (dfpypy), has also attracted attention for deep blue Ir(III) complexes.[4] Compared with FIrpic, the $(dfpypy)_2Ir(pic)$ emission was shifted to blue region at 457 nm due to the electron deficiency of pyridine ring.

In addition, good ancillary ligand will greatly enhance photoluminescent properties of Ir(III) complexes and benefit their OLEDs performances. Our group reported Htpip (tetraphenylimidodiphosphinate acid) derivatives as ancillary ligands, which have two diphenyl phosphoryl ($Ph_2P{=}O$) groups, for efficient devices.[5] It is well known that $Ph_2P{=}O$ unit has been widely used to construct electron transport and ambipolar host materials due to its strongly electron-deficient nature with improved electron injecting and transporting property.[6] When $Ph_2P{=}O$ unit was introduced in the ancillary ligand, not only the charge transport ability of the complexes be improved, the four bulky

State Key Laboratory of Coordination Chemistry, Collaborative Innovation Center of Advanced Microstructures, Collaborative Innovation Center of Chemistry for Life Sciences, School of Chemistry and Chemical Engineering, Nanjing University, Nanjing 210093, P. R. China. E-mail: yxzheng@nju.edu.cn

† Electronic supplementary information (ESI) available. CCDC 1062396 and 1062397. For ESI and crystallographic data in CIF or other electronic format see DOI: 10.1039/c5ra14837e

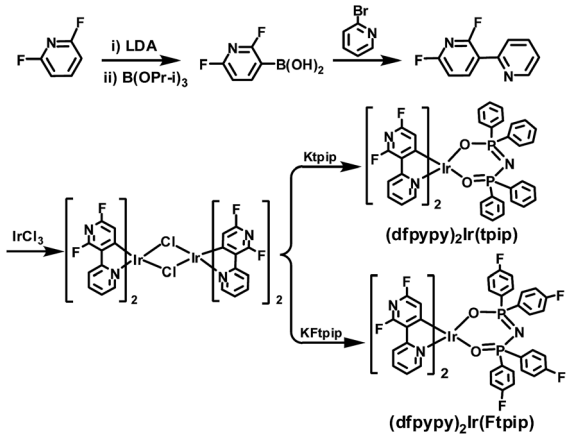

Scheme 1 Synthetic routes of ligands and complexes.

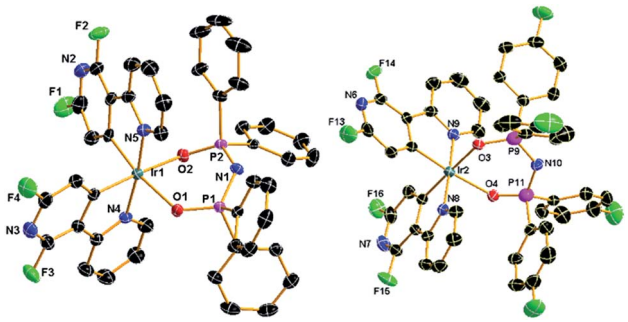

Fig. 1 Oak Ridge thermal ellipsoidal plot (ORTEP) diagrams of the complexes $(dfpypy)_2Ir(tpip)$ (left, CCDC: 1062396) and $(dfpypy)_2$-Ir(Ftpip) (right, CCDC: 1062397). Hydrogen atoms are omitted for clarity. Ellipsoids are drawn at 30% probability level.

phenyl groups also lead to a larger spatial separation of the neighboring molecules of the Ir(III) complexes to supress triplet–triplet annihilation (TTA) and triplet-polaron annihilation (TPA) effects. Therefore, the OLEDs with this kind of iridium emitters exhibited excellent high current efficiency and low efficiency roll-off. Herein, using dfpypy as the main ligand and tpip derivatives as the ancillary ligands, two iridium complexes ($(dfpypy)_2Ir(tpip)$ and $(dfpypy)_2Ir(Ftpip)$ (Ftpip: tetra(4-fluorophenyl)imidodiphosphinate acid), Scheme 1) were synthesized, and their photoluminescence and device performances were studied.

Results and discussion

Preparation and characterization of compounds

Scheme 1 shows the chemical structures and synthetic routes for $(dfpypy)_2Ir(tpip)$ and $(dfpypy)_2Ir(Ftpip)$ complexes. The reaction of 2,6-difluoropyridine with LDA (lithium diisopropylamide), $B(OPr\text{-}i)_3$ (isopropyl borate) gave 2,6-difluoropyridinyl-3-boronic acid.[5b,7] The fluorinated bipyridine ligand was synthesized using a Suzuki coupling reaction from 2,6-difluoropyridinyl-3-boronic acid and 2-bromopyridine. Htpip, fluorinated HFtpip and their potassium salts (Ktpip, KFtpip) were prepared according to our previous publications.[5] $(dfpypy)_2Ir(tpip)$ and $(dfpypy)_2Ir(Ftpip)$ were purified by silica chromatography and vacuum sublimation. Both compounds were fully characterized by ^1H NMR, high resolution mass spectrometry and X-ray crystallography.

X-ray crystallography

Single crystals grown from vacuum sublimation further confirmed the molecular structures of $(dfpypy)_2Ir(tpip)$ and $(dfpypy)_2Ir(Ftpip)$. Fig. 1 shows the Oak Ridge thermal ellipsoidal plot (ORTEP)[8] diagrams of $(dfpypy)_2Ir(tpip)$ and $(dfpypy)_2Ir(Ftpip)$ given by X-ray analysis. Selected parameters of the molecular structures and atomic coordinates were collected in the Tables S1 and S2.† The iridium center adopts a distorted octahedral coordination geometry with two C^N cyclometalated ligands and one O^O ancillary ligand. For the two complexes, the bond lengths of Ir–C (1.965(5)–1.982(4) Å) and Ir–N (2.030(4)–2.048(3) Å) are within the range reported for the related complexes.[4a] However, the bond lengths of Ir–O for $(dfpypy)_2Ir(tpip)$ are somewhat longer than that of $(dfpypy)_2$-Ir(Ftpip), attributed to the inducement of withdrawing group fluorine in the ancillary ligand.

Thermal stability

The thermal stability of the emitters is important for the stable OLEDs. In this cases, the thermal properties of the two iridium complexes were characterized by differential scanning calorimetry (DSC) and thermogravimetric (TG) measurements under a nitrogen steam. From the DSC curves in Fig. 2 it can be observed the melting points of $(dfpypy)_2Ir(tpip)$ and $(dfpypy)_2$-Ir(Ftpip) are as high as 325 and 289 °C, respectively. The TG curves give the decomposition temperatures (5% loss of weight) as 420 °C for $(dfpypy)_2Ir(tpip)$ and 414 °C for $(dfpypy)_2Ir(Ftpip)$, respectively, indicating that the fluorine atoms at the tpip ligand will reduce the melting point effectively but will not affect their decomposition temperature obviously. And the high decomposition temperature of the complexes suggested they are suitable for application in OLEDs.

Photophysical and electrochemical property

The UV-vis absorption and emission spectra of the $(dfpypy)_2$-Ir(tpip), $(dfpypy)_2Ir(Ftpip)$ complexes are shown in Fig. 3 and the photophysical data are collected in Table 1. The absorption

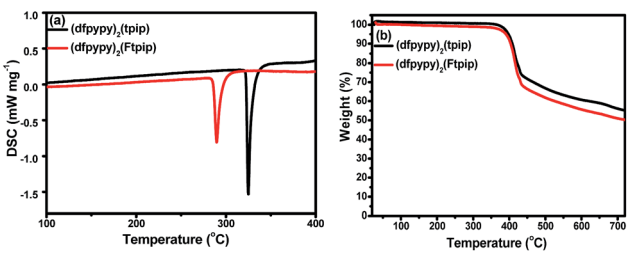

Fig. 2 The DSC (a) and TG (b) curves of $(dfpypy)_2Ir(tpip)$ and $(dfpypy)_2Ir(Ftpip)$ complexes.

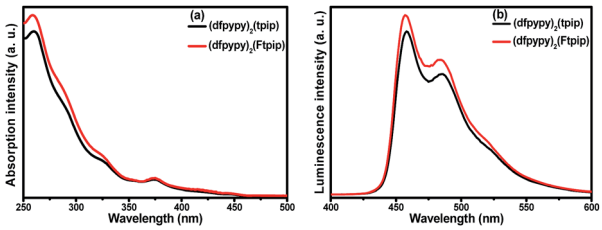

Fig. 3 The UV-vis absorption (a) and emission spectra (b) of complexes $(dfpypy)_2Ir(tpip)$ and $(dfpypy)_2Ir(Ftpip)$ in CH_2Cl_2 at room temperature.

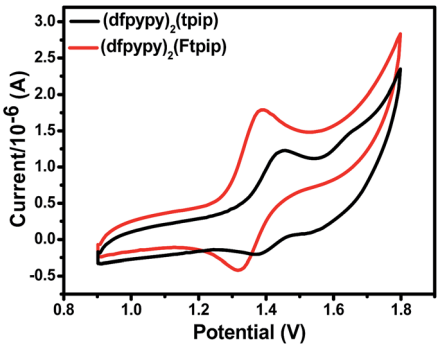

Fig. 4 Cyclic voltammograms of complexes $(dfpypy)_2Ir(tpip)$ and $(dfpypy)_2Ir(Ftpip)$.

spectra of these complexes show broad and intense bands below 320 nm, assigned to the spin-allowed intraligand ^{1}LC ($\pi \rightarrow \pi^*$) transition of cyclometalated main ligands and tpip type ligands. The weak bands extend to 520 nm maybe assigned to spin-allowed metal-ligand charge transfer band (^{1}MLCT), partially overlapped by the broad LC absorption and spin forbidden ^{3}MLCT transition bands caused by the large spin orbital coupling (SOC) that was introduced by Ir(III) center and an efficient spin–orbit coupling that is prerequisite for phosphorescent emission.

Both $(dfpypy)_2Ir(tpip)$ and $(dfpypy)_2Ir(Ftpip)$ show sky-blue phosphorescence in CH_2Cl_2 under the irradiation of UV light at room temperature. Excited at 370 nm, $(dfpypy)_2Ir(tpip)$ and $(dfpypy)_2Ir(Ftpip)$ show almost same emissions maxima at 457 nm with shoulders of 485 nm at room temperature, indicating that the introducing of fluorine in tpip have no obvious effect on the absorption and emission properties of the two complexes. And at 77 K, the two major peaks become sharper and the third shoulder peak is in evidence. According to literature,[4e] the emissions of our complexes are similar to that of $(dfpypy)_2Ir(acac)$. The maximum peaks generated from the electronic 0–0 transition between the lowest triplet excited state to the ground state. The emission at lower energy range might stem from overlapping vibrational satellites.[9] In general, the emission bands from MLCT states are broad and featureless, whereas a highly structured emission band mainly originates from the $^3\pi$–π^* state. Accordingly, all of the complexes emit from a mixture of MLCT states and the dominant ligand-based $^3\pi$–π^* state. This indicates that the MLCT characters involved in the emitting T_1 states of different complexes are various, but significant, since a dominant MLCT character in T_1 usually leads to large inhomogeneity and low-energy lying metal-ligand vibrational satellites, smearing out the spectrum below the electronic original emission.[10]

It is well known that the phosphorescence lifetime (τ_p) of the Ir(III) complex is a crucial factor that determines the rate of triplet–triplet annihilation (TTA) in the OLEDs. The long τ_p of the Ir(III) dopant usually causes serious TTA effect.[11] The lifetimes of complexes $(dfpypy)_2Ir(tpip)$ and $(dfpypy)_2Ir(Ftpip)$ are 1.83 μs and 1.90 μs (Table 1, Fig. S1†), respectively, measured in degassed CH_2Cl_2 (2×10^{-5} M) with a excitation of 370 nm at room temperature, which are indicative of the phosphorescent origin for the excited states in each case. The $(dfpypy)_2Ir(tpip)$ and $(dfpypy)_2Ir(Ftpip)$ quantum yields are 7.1% and 7.0%, respectively, measured using an integration sphere at room temperature in degassed CH_2Cl_2.

The redox properties and highest occupied molecular orbital (HOMO), lowest unoccupied molecular orbital (LUMO) energy levels of the dopants are relative to the charge transport ability and design of the OLED structure. To calculate the HOMO and LUMO energy levels of the complexes, cyclic voltammetry experiments were carried out using ferrocene as the internal standard (Fig. 4). During the anodic scan in CH_2Cl_2, $(dfpypy)_2Ir(tpip)$ and $(dfpypy)_2Ir(Ftpip)$ exhibit a reversible redox with the oxidation potential in the range of 1.39–1.46 V, attributed to the metal-centered Ir(III)/Ir(IV) redox couple.[12] Complex $(dfpypy)_2Ir(Ftpip)$ shows lower oxidation potential (1.39 V) than that of $(dfpypy)_2Ir(tpip)$ (Table 1), indicating the fluorine atoms in the tpip ancillary ligand make the complex easier be oxidated. The HOMO levels of the $(dfpypy)_2Ir(tpip)$ and $(dfpypy)_2Ir(Ftpip)$ complexes are −6.00 and −5.93 eV, respectively, calculated from the oxidation potentials. And the LUMO levels of them are −3.20 and −3.15 eV, respectively, obtained from the HOMOs and band gap obtained from UV-vis absorption spectra (Table 1).[13] The F atoms in the tpip increased the HOMO/LUMOs of the complexes.

Table 1 Photophysical data of $(dfpypy)_2Ir(tpip)$ and $(dfpypy)_2Ir(Ftpip)$

Complex	T_m/T_d[a] [°C]	λ_{Abs}[b] [nm]	$\lambda_{em,RT}$[b] [nm]	τ[b] [μs]	Φ_p[c] [%]	E_T[d]	E_{ox} [V]	HOMO/LUMO[e] [eV]
$(dfpypy)_2Ir(tpip)$	325/420	252/373	457/484	1.83	7.1	2.69	1.46	−6.00/−3.20
$(dfpypy)_2Ir(Ftpip)$	289/414	253/373	457/484	1.90	7.0	2.72	1.39	−5.93/−3.15

[a] T_m: melting temperature, T_d: decomposed temperature. [b] Absorption, emission spectra and lifetime were taken in degassed CH_2Cl_2 at room temperature. [c] Φ: emission quantum yields were measured using the integrating-sphere system. [d] Triplet energy level was calculated from the frozen phosphorescent spectra measured at 77 K. [e] From the onset of oxidation potentials of the cyclovoltammetry (CV) diagram using ferrocene as the internal standard and the optical band gap from the absorption spectra in degassed CH_2Cl_2.

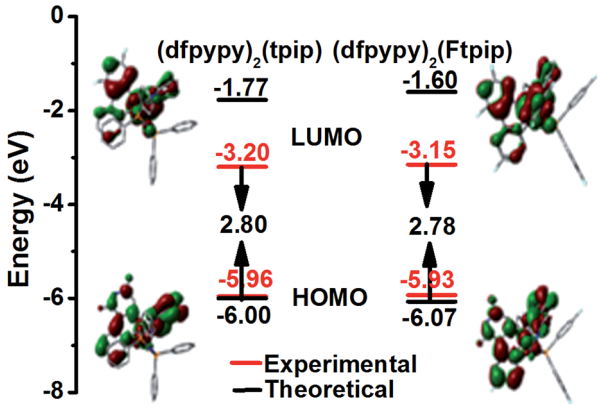

Fig. 5 MO patterns and energy diagram for $(dfpypy)_2Ir(tpip)$ and $(dfpypy)_2Ir(Ftpip)$.

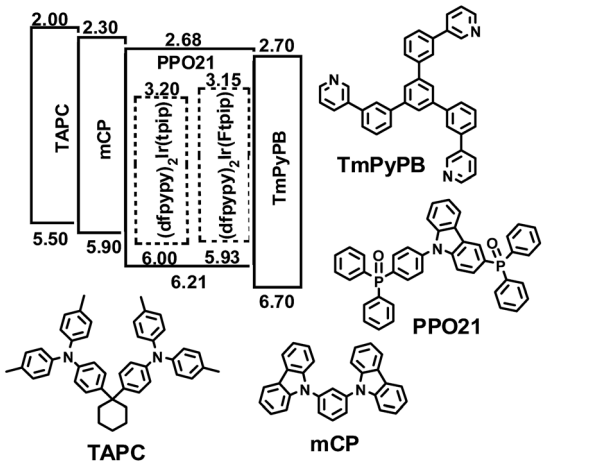

Scheme 2 The molecular structures of the materials and energy level diagrams of HOMO/LUMO levels of devices.

Theoretical calculation

The density functional theory (DFT) calculations for Ir(III) complexes were conducted to gain insights into the electronic states and the orbital distribution employing Gaussian09 software[14] with B3LYP functional.[15] The basis set used for C, H, N, O, F and P atoms was 6-31G(d,p) while the LanL2DZ basis set was employed for Ir atoms.[16] The CH_2Cl_2 solvent effect was taken into consideration using conductor like polarizable continuum model (C-PCM).[17] The relative energies of the HOMO/LUMO for complexes are shown in Fig. 5 and the orbital distributions are summarized in Table S3.† The results are helpful for the assignment of the electron transition characteristics and the discussion on the photophysical variations. For these complexes, the HOMOs correspond to a mixture of dfpypy group (35.36–37.36%) and Ir d orbitals (56.11–56.22%) with minor contributions from the tpip, Ftpip ligands (6.41–8.52%). While the LUMOs are mainly localized on the dfpypy (90.77–91.53%) with minor contributions from Ir d orbitals (5.02%) and tpip, Ftpip ligands (3.45–4.01%). Compared with $(dfpypy)_2Ir(tpip)$, the orbital distributions of HOMO/LUMO for $(dfpypy)_2Ir(Ftpip)$ have less contributions from Ir d orbitals and dfpypy ligand, more contributions from the Ftpip ligand, which indicated that the F atom affect the orbital distributions in some degree.

OLEDs performance

Since the HOMO levels of the two complexes are low (−6.00 and −5.93 eV, respectively), a bipolar host material of PPO21 (3-(diphenylphosphoryl)-9-(4-(diphenylphosphoryl)phenyl)-9*H*-carbazole) with low HOMO level (−6.21 eV) was used for complete energy transfer from the host to the dopant and good device performances.[18] The device named as **B1** using $(dfpypy)_2Ir(tpip)$ as the emitter as the example has a structure of ITO/TAPC (1,1-bis[4-(di-*p*-tolylamino)phenyl]cyclohexane, 40 nm)/$(dfpypy)_2$-Ir(tpip) (8 wt%): PPO21 (25 nm)/TmPyPB (1,3,5-tri(*m*-pyrid-3-yl-phenyl)benzene, 50 nm)/LiF (1 nm)/Al (100 nm). TAPC and TmPyPB[19] act as hole and electron transport materials, respectively. Scheme 2 shows the energy level diagrams of HOMO/LUMO levels (relative to vacuum level) for devices and materials. The device characteristics are shown in Fig. 6 and S3,† and the key EL data are summarized in Table 2.

For device **B1**, the optimal device performances are achieved at the doping level of 8 wt% with blue electroluminescence (EL) at 458 nm. As shown in Fig. 6, the EL spectrum is very close to the PL spectrum of the $(dfpypy)_2Ir(tpip)$ in CH_2Cl_2 solution indicating that the EL originates from the triplet excited states of the Ir(III) complex. No emission from the host material suggests that the energy and/or charge transfer from the host exciton to the phosphor is complete upon electrical excitation. The turn-on voltage of **B1** is 3.4 V with a maximum current efficiency ($\eta_{c,max}$) of 5.74 cd A^{-1} and a maximum external quantum efficiency (EQE) of 3.7% at 6.2 V, a maximum power efficiency ($\eta_{p,max}$) of 3.19 lm W^{-1} at 5.0 V and a maximum luminance (L_{max}) of 4805 cd m^{-2}.

The device efficiency and luminance are lower compared with the reported device results based on $Ir(dfpypy)_3$, $(dfpypy)_2Ir(pic)$ and $(dfpypy)_2Ir(acac)$.[4] For device **B1**, although the energy levels of host and $(dfpypy)_2Ir(tpip)$ are match, the energy barrier from the hole transport layer TAPC to the host material PPO21 is too large ($\Delta E = 0.31$ eV), which make against the hole injection and confinement in the emissive layer, leading to low efficiency and luminance. Therefore, to lower the HOMO energy barrier between TAPC/PPO21 and improve the device performances, a 10 nm mCP was inserted as a "ladder" between the TAPC and PPO21 layers to decrease the energy barrier due to its suitable HOMO level (−5.90 eV). The devices with the structure of ITO/TAPC (40 nm)/mCP (10 nm)/$(dfpypy)_2Ir(tpip)$ or $(dfpypy)_2Ir(Ftpip)$ (8 wt%): PPO21 (25 nm)/TmPyPB (50 nm)/LiF (1 nm)/Al (100 nm) were named **B2** and **B3**, respectively. The low-lying HOMO level (−6.70 eV) and high triplet energy level (2.78 eV) of TmPyPB will block the hole and achieve a well confinement of hole within the emissive layer. Moreover, the small energy barrier (0.02 eV) between TmPyPB and PPO21 will make it easy for electron transport to the emissive layer.

Compared with device **B1**, device **B2** with same emitter displays much higher performances. The maximum luminance

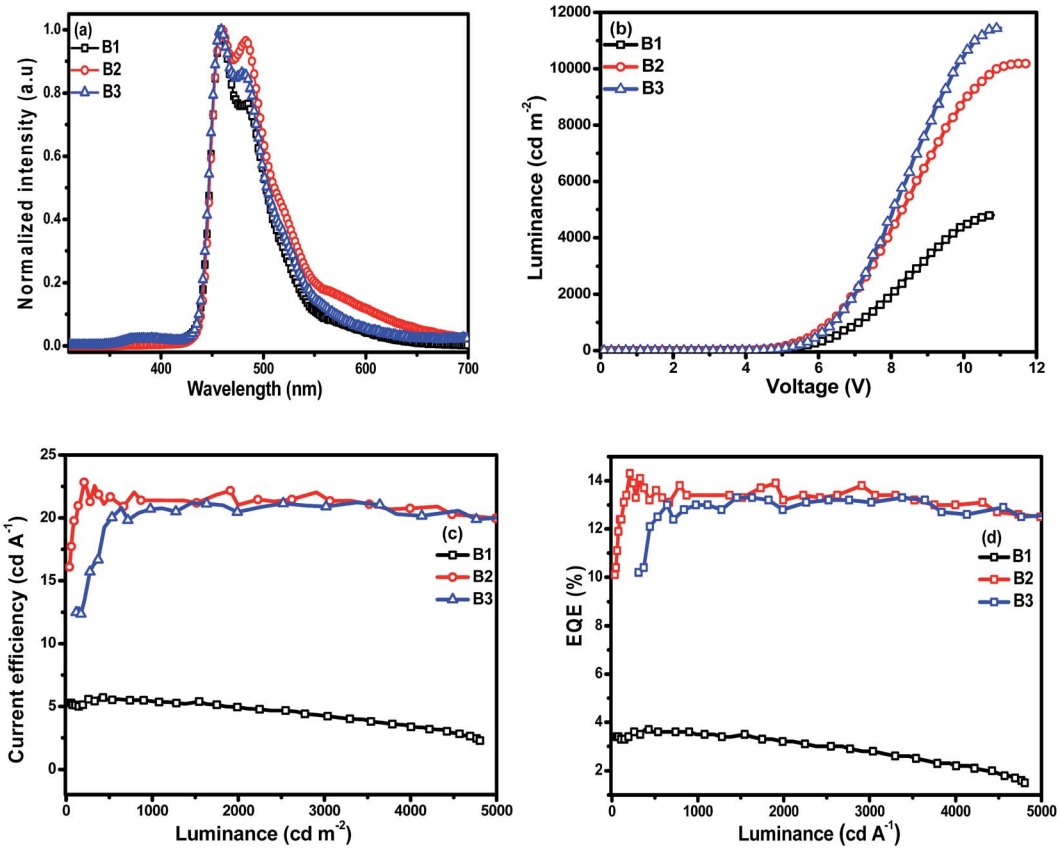

Fig. 6 Characteristics of devices of **B1**, **B2** and **B3** with configuration ITO/TAPC (40 nm)/mCP (10 nm)/$(dfpypy)_2Ir(tpip)$ or $(dfpypy)_2Ir(Ftpip)$ (8 wt%): PPO21 (25 nm)/TmPyPB (50 nm)/LiF (1 nm)/Al (100 nm): (a) electroluminescence spectra; (b) luminance–voltage (*L*–*V*) curves; (c) current efficiency–luminance (η_c–*L*) curves; (d) external quantum efficiency–luminance (EQE–*L*) curves.

Table 2 EL performances of the devices **B1**–**B3**

Device	Emitter	$V_{turn\text{-}on}$ [a] (V)	L_{max} [b] (voltage) [cd m^{-2} (V)]	$\eta_{c,max}$ [c] (voltage) [cd A^{-1} (V)]	$\eta_{c,L1000}$ [d]	$\eta_{c,L5000}$ [d]	EQE_{max} [e] [%]	$\eta_{p,max}$ [f] (voltage) [lm W^{-1} (V)]	CIE (*x*, *y*)
B1	$(dfpypy)_2Ir(tpip)$	3.4	4805(10.8)	5.74(6.2)	5.34	—	3.7	3.19(5.0)	0.16, 0.21
B2	$(dfpypy)_2Ir(tpip)$	3.8	10 182(11.5)	22.83(5.2)	20.39	19.95	14.3	13.87(5.2)	0.19, 0.28
B3	$(dfpypy)_2Ir(Ftpip)$	3.7	11 406(10.8)	20.79(6.1)	20.75	20.08	13.0	10.70(6.1)	0.17, 0.22

[a] $V_{turn\text{-}on}$: turn-on voltage recorded at a luminance of 1 cd m^{-2}. [b] L_{max}: maximum luminance. [c] $\eta_{c,max}$: maximum current efficiency. [d] $\eta_{c,L1000}$, $\eta_{c,L5000}$: the current efficiency obtained at 1000 and 5000 cd m^{-2} respectively. [e] EQE_{max}: maximum external quantum efficiency. [f] $\eta_{p,max}$: maximum power efficiency.

was improved to 10 182 cd m^{-2}, the current efficiency was increased to 22.83 cd A^{-1} together with a maximum EQE of 14.3%, and the maximum power efficiency reached to 13.7 lm W^{-1} at 5.2 V. The results suggest that the optimization of the device structure leads to a more effectively triplet exciton confinement and charge balance in the emitting layer. Device **B3** using $(dfpypy)_2Ir(Ftpip)$ also show similar performances with a maximum current efficiency of 20.79 cd A^{-1}, a maximum EQE of 13.0% and a maximum power efficiency of 10.76 lm W^{-1}. The introducing of fluorine in the ancillary ligand tpip have no much effect on the characters of the OLED. The device efficiencies are comparative to that using other dfpypy based complexes.[4] However, from the current efficiency–luminance (η_c–*L*) and external quantum efficiency–luminance (EQE–*L*) curves it can be observed that the efficiency roll-off ratios of devices **B2** and **B3** are mild, which are useful for practical application. For example, at 100 cd m^{-2} brightness for display, the current efficiencies of devices **B2** and **B3** are 19.78, 13.74 cd A^{-1}, respectively. At 1000 cd m^{-2} brightness for light, these values are still 20.39 and 20.75 cd A^{-1}, respectively. Even at the high luminance of 5000 cd m^{-2}, these data are also kept at 19.95 and 20.08 cd A^{-1}, respectively.

Conclusions

Two blue-emitting iridium complexes, $(dfpypy)_2Ir(tpip)$ and $(dfpypy)_2Ir(Ftpip)$, containing fluorinated substituted bipyridine as the main ligand and tetraphenylimidodiphosphinate derivatives as the ancillary ligands were prepared. PHOLEDs fabricated with the structure of ITO/1,1-bis[4-(di-*p*-tolylamino)phenyl]cyclohexane (TAPC, 40 nm)/1,3-bis(9*H*-carbazol-9-yl)benzene (mCP, 10 nm)/$(dfpypy)_2Ir(tpip)$ or $(dfpypy)_2Ir(Ftpip)$ (8 wt%): 3-(diphenylphosphoryl)-9-(4-(diphenylphosphoryl)phenyl)-9*H*-carbazole (PPO21, 25 nm)/1,3,5-tri(*m*-pyrid-3-yl-phenyl)benzene (TmPyPB, 50 nm)/LiF (1 nm)/Al (100 nm) showed maximum current efficiency (η_c) values as 22.83 and 20.79 cd A^{-1}, maximum external quantum efficiency as 14.3% and 13.0% with low efficiency roll-off, respectively, which proves that these complexes have potential application as the efficient blue emitters in OLEDs.

Experimental section

Materials and measurements

Htpip, HFtpip and their potassium salts (Ktpip, KFtpip) were synthesized according our former publications.[5] All reagents and chemicals were purchased from commercial sources and used without further purification. ^{1}H NMR spectra were measured on a Bruker AM 500 spectrometer. Mass spectra (MS) were obtained with an ESI-MS (LCQ Fleet, Thermo Fisher Scientific). High resolution mass spectra (HR EI-MS) were recorded from Agilent 6540 UHD Accurate-Mass Q-TOF LC/MS. Absorption and photoluminescence spectra were measured on a UV-3100 spectrophotometer and a Hitachi F-4600 photoluminescence spectrophotometer, respectively. The decay lifetimes and absolute photoluminescent quantum yields were measured with an Edinburgh Instrument FLS-920 fluorescence spectrometer equipped with an integrating sphere in degassed CH_2Cl_2 solution at room temperature. Cyclic voltammetry measurements were conducted on a MPI-A multifunctional electro-chemical and chemiluminescent system (Xi'an Remex Analytical Instrument Ltd Co., China) at room temperature with a polished Pt plate as the working electrode, platinum thread as the counter electrode and Ag–$AgNO_3$ (0.1 M) in CH_3CN as the reference electrode, tetra-*n*-butylammonium perchlorate (0.1 M) was used as the supporting electrolyte, using Fc^+/Fc as the internal standard, the scan rate was 0.1 V s^{-1}.

X-ray crystallography

X-ray crystallography of the single crystals of the complexes were carried out on a Bruker SMART CCD diffractometer using monochromated Mo Ka radiation (λ = 0.71073 Å) at room temperature. Cell parameters were retrieved using SMART software and refined using SAINT[20] on all observed reflections. Data were collected using a narrow-frame method with scan widths of 0.301 in o and an exposure time of 10 s per frame. The highly redundant data sets were reduced using SAINT and corrected for Lorentz and polarization effects. Absorption corrections were applied using SADABS[21] supplied by Bruker. The structures were solved by direct methods and refined by full-matrix least-squares on F^2 using the program SHELXS-97.[22] The positions of metal atoms and their first coordination spheres were located from direct-methods E-maps; other non-hydrogen atoms were found in alternating difference Fourier syntheses and least-squares refinement cycles and during the final cycles refined anisotropically. Hydrogen atoms were placed in calculated position and refined as riding atoms with a uniform value of Uiso.

OLEDs fabrication and measurement

All OLEDs were fabricated on the pre-patterned ITO-coated glass substrate with a sheet resistance of 15 Ω sq^{-1}. All chemicals used for EL devices were sublimed in vacuum (2.2×10^{-4} Pa) prior to use. The deposition rate for organic compounds is 1–2 Å s^{-1}. The phosphors and PPO21 host were co-evaporated to form the 25 nm emitting layer from two separate sources. The cathode consisting of LiF/Al was deposited by the evaporation of LiF with a deposition rate of 0.1 Å s^{-1} and then by evaporation of Al metal with a rate of 3 Å s^{-1}. The characteristics of the devices were measured with a computer controlled KEITHLEY 2400 source meter with a calibrated silicon diode in air without device encapsulation. On the basis of the uncorrected PL and EL spectra, the CIE coordinates were calculated using a test program of the spectra scan PR650 spectrophotometer.

General syntheses of ligands

A stirred solution of LDA (lithium diisopropylamide, 2 M, 5.17 mL, 10.35 mmol) in diethyl ether (30 mL) was cooled to −60 °C. 2,6-Difluoropyridine (1 g, 8.6 mmol) was injected dropwise into the cool solution over 15 min. One hour later, $B(OPr\text{-}i)_3$ (2.38 mL, 10.35 mmol) was added and the mixture was kept at −60 °C for one hour. After the reaction mixture was warmed to room temperature slowly and concentrated under reduced pressure, the pH was adjusted to 10 by the slow addition of aqueous NaOH solution (1 M, 20 mL). The aqueous layer was separated and the organic phase was extracted with one portion water. The combined water phase was acidified to pH = 4 by the dropwise addition of 2 N HCl. Extraction with ethyl acetate and evaporation of the solvent gave the crude (2,6-difluoropyridin-3-yl) boronic acid. 2-Bromopyridine (1 mL, 10 mmol), tetrakis (triphenylphosphine)palladium^0 (0.34 g, 0.3 mmol) and the boronic acids (10 mmol) were added in 50 mL THF. After 20 mL of aqueous 2 N K_2CO_3 was delivered, the reaction mixture was heated at 70 °C for 1 day under nitrogen. The mixture was poured into water and extracted with CH_2Cl_2 (10 mL × 3 times). Finally silica column purification (*n*-hexane : EtOAc = 7 : 1 as eluant) gave colorless solid 2′,6′-difluoro-2,3′-bipyridine (dfpypy) with a yield of 60%. ^{1}H NMR (500 MHz, $CDCl_3$): δ 8.57 (m, 2H), 7.69 (m, 2H), 7.18 (m, 1H), 6.87 (m, 1H). MS(ESI): calcd: *m*/*z* 192.05 for $[M]^+$ ($C_{10}H_6F_2N_2$), found: *m*/*z* 293.25 $[M + H]^+$.

General syntheses of iridium complexes. A mixture of $IrCl_3 \cdot nH_2O$ (0.78 g, 4.00 mmol) and dfpypy (0.57 g, 1.62 mmol) in 2-ethoxyethanol/water (10 mL, 1 : 1, v/v) was refluxed for 24 h. After cooling, the yellow solid precipitate was filtered to give the crude cyclometalated Ir(III) chloro-bridged dimer (0.55 g, 0.4 mmol). Then the slurry of crude chloro-bridged dimer (0.4

mmol) and Ktpip or KFtpip (0.8 mmol) in 2-ethoxyethanol (20 mL) was refluxed for 24 h. The solvent was evaporated at low pressure and the crude product was washed by water, and then chromatographed using CH_2Cl_2 as eluant gave the corresponding complexes, which were further purified by sublimation in vacuum.

(dfpypy)$_2$Ir(tpip). Yield: 40%. ^{1}H NMR (500 MHz, $CDCl_3$) δ 8.99 (d, J = 5.6 Hz, 2H), 8.08 (d, J = 8.2 Hz, 2H), 7.79 (dd, J = 12.4, 7.8 Hz, 4H), 7.58 (t, J = 7.9 Hz, 2H), 7.50–7.25 (m, 11H), 7.18 (t, J = 7.4 Hz, 2H), 7.01 (dd, J = 10.5, 4.4 Hz, 4H), 6.75 (dd, J = 7.2, 6.0 Hz, 2H), 5.55 (s, 2H). ESI-MS: 992.33 $[M + H]^+$. HR EI-MS calcd: m/z 991.1440 for $[M]^+$ ($C_{44}H_{30}F_4IrN_5O_2P_2$), found: m/z 992.1517 $[M + H]^+$.

(dfpypy)$_2$Ir(Ftpip). Yield: 36%. ^{1}H NMR (500 MHz, $CDCl_3$) δ 8.90 (d, J = 5.7 Hz, 2H), 8.12 (d, J = 8.2 Hz, 2H), 7.74 (ddd, J = 43.5, 13.9, 7.1 Hz, 6H), 7.27 (ddd, J = 12.0, 6.8, 4.0 Hz, 4H), 7.10 (t, J = 8.5 Hz, 4H), 6.83 (t, J = 6.4 Hz, 2H), 6.71 (t, J = 8.6 Hz, 4H), 5.53 (s, 2H). ESI-MS: 1064.08 $[M + H]^+$. HR EI-MS calcd: m/z 1063.1063 for $[M]^+$ ($C_{44}H_{26}F_8IrN_5O_2P_2$), found: m/z 1064.1138 $[M + H]^+$.

Acknowledgements

This work was supported by the National Natural Science Foundation of China (21371093, 91433113, 21401099), the Major State Basic Research Development Program (2011CB808704, 2013CB922101) and the Natural Science Foundation of Jiangsu Province (BK20130054).

Notes and references

1 (*a*) S. Lamansky, P. Djurovich, D. Murphy, F. Abdel-Razzaq, H. E. Lee, C. Adachi, P. E. Burrows, S. R. Forrest and M. E. Thompson, *J. Am. Chem. Soc.*, 2001, **123**, 4304; (*b*) J. J. Kim, Y. You, Y.-S. Park, J.-J. Kim and S. Y. Park, *J. Mater. Chem.*, 2009, **19**, 8347; (*c*) Z.-Q. Chen, Z.-Q. Bian and C.-H. Huang, *Adv. Mater.*, 2010, **22**, 1534; (*d*) S. Chen, G. Tan, W.-Y. Wong and H.-S. Kwok, *Adv. Funct. Mater.*, 2011, **21**, 3785; (*e*) C.-H. Fan, P. Sun, T.-H. Su and C.-H. Cheng, *Adv. Mater.*, 2011, **23**, 2981; (*f*) J. M. Fernandez-Hernandez, C.-H. Yang, J. I. Beltran, V. Lemaur, F. Polo, R. Froehlich, J. Cornil and L. de Cola, *J. Am. Chem. Soc.*, 2011, **133**, 10543; (*g*) K.-Y. Lu, H.-H. Chou, C.-H. Hsieh, Y.-H. O. Yang, H.-R. Tsai, H.-Y. Tsai, L.-C. Hsu, C.-Y. Chen, I. C. Chen and C.-H. Cheng, *Adv. Mater.*, 2011, **23**, 4933; (*h*) H.-H. Chou, Y.-K. Li, Y.-H. Chen, C.-C. Chang, C.-Y. Liao and C.-H. Cheng, *ACS Appl. Mater. Interfaces*, 2013, **5**, 6168; (*i*) H. Sasabe and J. Kido, *Eur. J. Org. Chem.*, 2013, **2013**, 7653; (*j*) H. Sasabe, H. Nakanishi, Y. Watanabe, S. Yano, M. Hirasawa, Y.-J. Pu and J. Kido, *Adv. Funct. Mater.*, 2013, **23**, 5550; (*k*) X. Yang, N. Sun, J. Dang, Z. Huang, C. Yao, X. Xu, C.-L. Ho, G. Zhou, D. Ma, X. Zhao and W.-Y. Wong, *J. Mater. Chem. C*, 2013, **1**, 3317; (*l*) H. Cao, H. Sun, Y. Yin, X. Wen, G. Shan, Z. Su, R. Zhong, W. Xie, P. Li and D. Zhu, *J. Mater. Chem. C*, 2014, **2**, 2150; (*m*) A. Graf, P. Liehm, C. Murawski, S. Hofmann, K. Leo and M. C. Gather, *J. Mater. Chem. C*, 2014, **2**, 10298; (*n*) V. K. Rai, M. Nishiura, M. Takimoto and Z. Hou, *J. Mater. Chem. C*, 2014, **2**, 5317; (*o*) X. Xu, X. Yang, J. Dang, G. Zhou, Y. Wu, H. Li and W.-Y. Wong, *Chem. Commun.*, 2014, **50**, 2473; (*p*) X. Yang, G. Zhou and W.-Y. Wong, *J. Mater. Chem. C*, 2014, **2**, 1760.

2 R. J. Holmes, S. R. Forrest, Y. J. Tung, R. C. Kwong, J. J. Brown, S. Garon and M. E. Thompson, *Appl. Phys. Lett.*, 2003, **82**, 2422.

3 (*a*) S. J. Yeh, M. F. Wu, C. T. Chen, Y. H. Song, Y. Chi, M. H. Ho, S. F. Hsu and C. H. Chen, *Adv. Mater.*, 2005, **17**, 285; (*b*) S.-Y. Takizawa, H. Echizen, J.-I. Nishida, T. Tsuzuki, S. Tokito and Y. Yamashita, *Chem. Lett.*, 2006, **35**, 748; (*c*) C.-H. Yang, Y.-M. Cheng, Y. Chi, C.-J. Hsu, F.-C. Fang, K.-T. Wong, P.-T. Chou, C.-H. Chang, M.-H. Tsai and C.-C. Wu, *Angew. Chem., Int. Ed.*, 2007, **46**, 2418; (*d*) Y. Zheng, S.-H. Eom, N. Chopra, J. Lee, F. So and J. Xue, *Appl. Phys. Lett.*, 2008, **92**, 223301; (*e*) S. H. Kim, J. Jang, S. J. Lee and J. Y. Lee, *Thin Solid Films*, 2008, **517**, 722; (*f*) H.-J. Seo, K.-M. Yoo, M. Song, J. S. Park, S.-H. Jin, Y. I. Kim and J.-J. Kim, *Org. Electron.*, 2010, **11**, 564; (*g*) S. Lee, S.-O. Kim, H. Shin, H.-J. Yun, K. Yang, S.-K. Kwon, J.-J. Kim and Y.-H. Kim, *J. Am. Chem. Soc.*, 2013, **135**, 14321; (*h*) J.-B. Kim, S.-H. Han, K. Yang, S.-K. Kwon, J.-J. Kim and Y.-H. Kim, *Chem. Commun.*, 2015, **51**, 58.

4 (*a*) S. J. Lee, K.-M. Park, K. Yang and Y. Kang, *Inorg. Chem.*, 2009, **48**, 1030; (*b*) N. Jung, E. Lee, J. Kim, H. Park, K.-M. Park and Y. Kang, *Bull. Korean Chem. Soc.*, 2012, **33**, 183; (*c*) F. Kessler, R. D. Costa, D. Di Censo, R. Scopelliti, E. Orti, H. J. Bolink, S. Meier, W. Sarfert, M. Graetzel, M. K. Nazeeruddin and E. Baranoff, *Dalton Trans.*, 2012, **41**, 180; (*d*) C.-H. Yang, M. Mauro, F. Polo, S. Watanabe, I. Muenster, R. Froehlich and L. de Cola, *Chem. Mater.*, 2012, **24**, 3684; (*e*) Y. Kang, Y.-L. Chang, J.-S. Lu, S.-B. Ko, Y. Rao, M. Varlan, Z.-H. Lu and S. Wang, *J. Mater. Chem. C*, 2013, **1**, 441; (*f*) S. B. Meier, W. Sarfert, J. M. Junquera-Hernandez, M. Delgado, D. Tordera, E. Orti, H. J. Bolink, F. Kessler, R. Scopelliti, M. Graetzel, M. K. Nazeeruddin and E. Baranoff, *J. Mater. Chem. C*, 2013, **1**, 58; (*g*) H. Oh, K.-M. Park, H. Hwang, S. Oh, J. H. Lee, J.-S. Lu, S. Wang and Y. Kang, *Organometallics*, 2013, **32**, 6427; (*h*) N. Darmawan, C.-H. Yang, M. Mauro, R. Froehlich, L. de Cola, C.-H. Chang, Z.-J. Wu and C.-W. Tai, *J. Mater. Chem. C*, 2014, **2**, 2569; (*i*) S. Oh, N. Jung, J. Lee, J. Kim, K.-M. Park and Y. Kang, *Bull. Korean Chem. Soc.*, 2014, **35**, 3590.

5 (*a*) Y.-C. Zhu, L. Zhou, H.-Y. Li, Q.-L. Xu, M.-Y. Teng, Y.-X. Zheng, J.-L. Zuo, H.-J. Zhang and X.-Z. You, *Adv. Mater.*, 2011, **23**, 4041; (*b*) M.-Y. Teng, S. Zhang, S.-W. Jiang, X. Yang, C. Lin, Y.-X. Zheng, L. Wang, D. Wu, J.-L. Zuo and X.-Z. You, *Appl. Phys. Lett.*, 2012, 100; (*c*) C.-C. Wang, Y.-M. Jing, T.-Y. Li, Q.-L. Xu, S. Zhang, W.-N. Li, Y.-X. Zheng, J.-L. Zuo, X.-Z. You and X.-Q. Wang, *Eur. J. Inorg. Chem.*, 2013, **2013**, 5683; (*d*) J. Wang, J. Liu, S. Huang, X. Wu, X. Shi, C. Chen, Z. Ye, J. Lu, Y. Su, G. He and Y. Zheng, *Org. Electron.*, 2013, **14**, 2854; (*e*) J. Wang, J. Liu, S. Huang, X. Wu, X. Shi, G. He and Y. Zheng, *Org. Electron.*, 2013, **14**, 2682; (*f*) Q.-L. Xu, C.-C. Wang, T.-Y. Li, M.-Y. Teng, S. Zhang, Y.-M. Jing, X. Yang, W.-N. Li, C. Lin,

Y.-X. Zheng, J.-L. Zuo and X.-Z. You, *Inorg. Chem.*, 2013, **52**, 4916; (*g*) M.-Y. Teng, S. Zhang, Y.-M. Jin, T.-Y. Li, X. Liu, Q.-L. Xu, C. Lin, Y.-X. Zheng, L. Wang and J.-L. Zuo, *Dyes Pigm.*, 2014, **105**, 105; (*h*) Q.-L. Xu, X. Liang, S. Zhang, Y.-M. Jing, X. Liu, G.-Z. Lu, Y.-X. Zheng and J.-L. Zuo, *J. Mater. Chem. C*, 2015, **3**, 3694.

6 (*a*) H.-H. Chou and C.-H. Cheng, *Adv. Mater.*, 2010, **22**, 2468; (*b*) S. O. Jeon, S. E. Jang, H. S. Son and J. Y. Lee, *Adv. Mater.*, 2011, **23**, 1436.

7 S. W. Magennis, S. Parsons and Z. Pikramenou, *Chem.–Eur. J.*, 2002, **8**, 5761.

8 L. J. Farrugia, *J. Appl. Crystallogr.*, 1997, **30**, 365.

9 A. F. Rausch, M. E. Thompson and H. Yersin, *Inorg. Chem.*, 2009, **48**, 1928.

10 (*a*) A. P. Wilde and R. J. Watts, *J. Phys. Chem.*, 1991, **95**, 622; (*b*) M. G. Colombo, T. C. Brunold, T. Riedener, H. U. Gudel, M. Fortsch and H. B. Burgi, *Inorg. Chem.*, 1994, **33**, 545.

11 (*a*) M. A. Baldo, C. Adachi and S. R. Forrest, *Phys. Rev. B: Condens. Matter Mater. Phys.*, 2000, **62**, 10967; (*b*) E. B. Namdas, A. Ruseckas, I. D. W. Samuel, S. C. Lo and P. L. Burn, *Appl. Phys. Lett.*, 2005, **86**, 091104.

12 S. Bettington, M. Tavasli, M. R. Bryce, A. Beeby, H. Al-Attar and A. P. Monkman, *Chem.–Eur. J.*, 2007, **13**, 1423.

13 (*a*) R. S. Ashraf, M. Shahid, E. Klemm, M. Al-Ibrahim and S. Sensfuss, *Macromol. Rapid Commun.*, 2006, **27**, 1454; (*b*) M. Thelakkat and H. W. Schmidt, *Adv. Mater.*, 1998, **10**, 219.

14 M. J. Frisch, G. W. Trucks, H. B. Schlegel, G. E. Scuseria, M. A. Robb, J. R. Cheeseman, G. Scalmani, V. Barone, B. Mennucci, G. A. Petersson, H. Nakatsuji, M. Caricato, X. Li, H. P. Hratchian, A. F. Izmaylov, J. Bloino, G. Zheng, J. L. Sonnenberg, M. Hada, M. Ehara, K. Toyota, R. Fukuda, J. Hasegawa, M. Ishida, T. Nakajima, Y. Honda, O. Kitao, H. Nakai, T. Vreven, J. A. Montgomery Jr, J. E. Peralta, F. Ogliaro, M. Bearpark, J. J. Heyd, E. Brothers, K. N. Kudin, V. N. Staroverov, R. Kobayashi, J. Normand, K. Raghavachari, A. Rendell, J. C. Burant, S. S. Iyengar, J. Tomasi, M. Cossi, N. Rega, J. M. Millam, M. Klene, J. E. Knox, J. B. Cross, V. Bakken, C. Adamo, J. Jaramillo, R. Gomperts, R. E. Stratmann, O. Yazyev, A. J. Austin, R. Cammi, C. Pomelli, J. W. Ochterski, R. L. Martin, K. Morokuma, V. G. Zakrzewski, G. A. Voth, P. Salvador, J. J. Dannenberg, S. Dapprich, A. D. Daniels, O. Farkas, J. B. Foresman, J. V. Ortiz, J. Cioslowski and D. J. Fox, *(GAUSSIAN 09, Revision A.01)*, Gaussian, Inc, Wallingford, CT, 2009.

15 (*a*) P. J. Hay, *J. Phys. Chem. A*, 2002, **106**, 1634; (*b*) A. D. Becke, *J. Chem. Phys.*, 1993, **98**, 5648; (*c*) C. T. Lee, W. T. Yang and R. G. Parr, *Phys. Rev. B: Condens. Matter Mater. Phys.*, 1988, **37**, 785.

16 S. Chiodo, N. Russo and E. Sicilia, *J. Chem. Phys.*, 2006, 125.

17 M. Cossi, N. Rega, G. Scalmani and V. Barone, *J. Comput. Chem.*, 2003, **24**, 669.

18 P. M. Borsenberger, L. Pautmeier, R. Richert and H. Bassler, *J. Chem. Phys.*, 1991, **94**, 8276.

19 S.-J. Su, T. Chiba, T. Takeda and J. Kido, *Adv. Mater.*, 2008, **20**, 2125.

20 *SAINT-Plus, version 6.02, Bruker Analytical X-ray System*, Madison, WI, 1999.

21 G. M. Sheldrick, *SADABS An empirical absorption correction program, Bruker Analytical X-ray Systems*, Madison, WI, 1996.

22 G. M. Sheldrick, *SHELXTL-97*, Universität of Göttingen, Göttingen, Germany, 1997.